Available online at www.sciencedirect.com
ScienceDirect
Electrochimica Acta 52 (2007) 2570–2579
ELECTROCHIMICA Acta
www.elsevier.com/locate/electacta

Investigation of corrosion behaviors of Mg–6Gd–3Y–0.4Zr alloy in NaCl aqueous solutions

Xing-Wu Guo [a,*], Jian-Wei Chang [a], Shang-Ming He [a], Wen-Jiang Ding [a], Xishu Wang [b]

[a] *School of Material Science and Engineering, National Engineering and Research Center for Light Alloy Net Forming (LAF), Shanghai Jiao Tong University, Shanghai 200030, China*
[b] *School of Aerospace, Tsinghua Uiversity, Beijing 100084, China*

Received 19 May 2006; received in revised form 30 August 2006; accepted 1 September 2006
Available online 11 October 2006

Abstract

The corrosion behaviors of Mg–6 wt.%Gd–3 wt.%Y–0.4 wt.%Zr (GW63K) alloy in 5 wt.% NaCl aqueous solutions have been investigated in both as-cast and T6 heat treatment conditions by immersion test and electrochemical techniques. The corrosion products and their morphologies formed in the solution after immersing various time have been analyzed by FE-SEM and XRD. It was found that the morphologies of the film of corrosion products varied with immersion time and changed from honeycomb into porous structure composed of tiny erect flaks after immersing 60 min. The phenomena of undermining and falling away of the noble second phase particles observed in the test can be used as an evidence to support the *Mechanism II* explaining the mechanism of negative difference effect (NDE) about magnesium and its alloys. It was indicated that the E_{CORR} of GW63K alloy in T6 condition (−1.71 V) is little nobler than that in as-cast (−1.73 V). It was shown by pitting scans that GW63K alloy has tendency to pit whether in as-cast or in T6 condition and the tendency in T6 condition is more serious than that in as-cast. An equivalent circuit was proposed based on the EIS experimental data and the honeycomb or porous characteristics of the corrosion products formed on the surface of GW63K alloy.

Keywords: Magnesium alloy; Heavy rare earth; Corrosion; Pitting; EIS

1. Introduction

Magnesium alloys containing heavy rare earth (HRE) elements are becoming more and more attractive due to their high strength and ductility. They have large potential applications as light structural materials for the aerospace and racing automotive industries. It has been reported that the recently developed Mg–Gd–Y alloys exhibit higher specific strength at both room and elevated temperatures and better creep resistance than conventional Al and Mg alloys, including WE54(Mg–5Y–2Nd–2HRE, wt.%), whose high temperature strength is the top of existing commercial magnesium alloys [1–8].

Many intensive and extensive fundamental investigations and evaluations about the corrosion problem of magnesium alloys have been carried out during the past decade [9–16]. It is becoming deeper and more comprehensive for people to comprehend the behaviors and mechanisms of the corrosion of magnesium alloys. However, most of these investigations devote their research works to the AZ(Mg–Al–Zn) and AM(Mg–Al–Mn) series of magnesium alloys, such as AZ91D and AM50. There were relatively few research reports to the magnesium alloys containing HRE. National Engineering and Research Center for Light Alloy Net Forming (LAF) is the largest and most important engineering research organization to research and development of magnesium alloys in China. The R&D of high performance magnesium alloys containing HRE elements has been carrying out in LAF during recent years. This work explores both the corrosion behaviors and the development process of the corrosion products of Mg–6Gd–3Y–0.4Zr (GW63K) alloy in NaCl 5 wt.% aqueous solutions in order to provide valuable corrosion behavior and electrochemical information that can help to understand the difference between the magnesium alloys containing HRE elements and non-containing HRE elements.

* Corresponding author. Tel.: +86 21 62932164; fax: +86 21 62932113.
E-mail address: xingwuguo@sjtu.edu.cn (X.-W. Guo).

0013-4686/$ – see front matter © 2006 Elsevier Ltd. All rights reserved.
doi:10.1016/j.electacta.2006.09.010

2. Experimental

2.1. Sample preparation

The chemical composition of GW63K alloy is 6 wt.%Gd, 3 wt.%Y, and 0.4 wt.%Zr. The small cylinder (Ø10 × 5) specimens of GW63K alloys used in this investigation in as-cast and T6 heat treatment conditions were prepared by wire cutting machine. The specimens were ground on Al_2O_3 waterproof abrasive paper, polished by manual polishing until scratches are removed, cleaned by rinsing with water, and then rinsed by ethanol and dried in air prior to immersion in the cell. The T6 heat treatment is that which solution treated at 500 °C for 6 h, quenched into hot water at ~80 °C, and then subsequently aged at 225 °C in an air furnace.

2.2. Immersion test

The main purpose of this test is to investigate the corrosion mechanism and to reveal the development and growth of corrosion products of GW63K alloy in NaCl aqueous solutions. To realize this purpose, six numbered small cylinder (Ø10 × 5) specimens of GW63K alloy in as-cast and T6 heat treatment conditions are immersed in NaCl 5 wt.% aqueous solutions contained in a 1 l beaker at the same time. The numbered specimen was taken out from the beaker one by one, respectively, after immersing a determined period of time, namely 10, 20 (or 30 min) and 60 min. They were cleaned by rinsing with pure water, and then rinsed by ethanol and dried in air prior to carry out FE-SEM and XRD analysis.

2.3. Apparatus for electrochemical test

The test cell used was the Model K47 corrosion cell system from Princeton Applied Research. The test electrode was a flat sample holder (K105) containing a small cylinder (Ø10 × 5) specimen of GW63K. Fig. 1 is an exploded view drawing of the K105 flat specimen holder. The two counter electrodes were high-density graphite. The reference electrode was a Saturated Calomel Electrode (SCE). The photograph of this system is shown in Fig. 2. The high-density graphite counter electrodes were on either side of the working electrode sample holder. The bridge tube incorporates a Vycor tip designed specifically to provide ultra low leakage rates with minimum IR drop through the tip. This arrangement eliminates complications arising from poisoning of test solutions by reference electrode filling solutions. All electrochemical measurements were carried out using a PARSTAT 2273 Potentiostat/Galvanostat controlled by a personal computer.

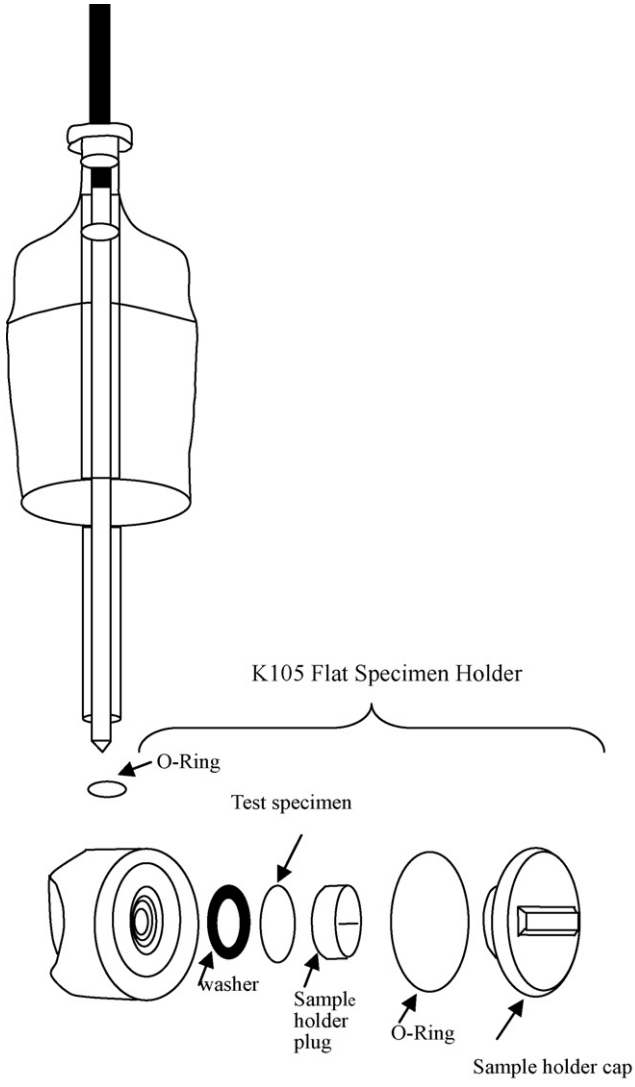

Fig. 1. Exploded view of K105 Flat Specimen Holder.

2.4. E_{CORR} (open circuit potential, OCP) versus time

Open circuit potential measurements (E_{CORR}) were made between the working electrode and the reference electrode without current being passed to the counter electrodes. This measurement showed the potential at which the anodic and cathodic reaction currents at the working electrode/solution interface were balanced. The experimental data can be used to characterize a test system so that the initial delay of other techniques can be specified in units of time rather than drift rate. In the case of GW63K corrosion, these measurements are very useful as qualitative information regarding the state of the working electrode surface. They were also used to evaluate the relative nobility of the specimens of GW63K in as-cast and T6 heat treatment conditions. E_{CORR} measurements were begun immediately after the specimen was immersed in the solution and they are made prior to electrochemical impedance spectroscopy (EIS) and cyclic polarization (Pitting Scans) experiments to ensure stability.

2.5. Electrochemical impedance spectroscopy (EIS)

The EIS measurements were carried out using the PowerSINE software of PARSTAT2273. It can perform EIS experiments from frequency ranges of 1 MHz to 10 uHz, via either potentiostatic control (Single-Sine, fast Multi-Sine, or Mott-Schottky), or galvanostatic control (Galvanostatic EIS). In this

Fig. 2. The photograph of the test cell.

work, the Single-Sine technique was used, the impedance measurements were carried out starting at an initial frequency of 100 kHz and stopping at a final frequency of 100 mHz. The AC perturbation amplitude was 10 mV and the number of points was 150. All the measurements of the present study were taken immediately after the open circuit potential measurements (E_{CORR}) were finished.

2.6. Cyclic polarization (pitting scans)

A cyclic polarization scan provides a qualitative view of pitting corrosion mechanisms and can determine the tendency of a material to undergo surface pitting or crevicing when placed in a specific corrosive environment. It is particularly useful in the development of magnesium alloys containing heavy rare earth (HRE) elements that require a high degree of pit resistance. The forward scanned polarization curves started from a cathodic potential of −0.25 V (versus E_{CORR}), namely E_I, where the surfaces of the alloys were not yet corroded, and extended to the vertex potential of 0.60 V (versus E_{CORR}), namely E_V. The forward scan is followed by a reverse scan back to the final potential −0.25 V (versus E_{CORR}), namely E_F. The scan rate is 2.5 mV/s, the step height is 1 mV. The schematic diagram of the waveform of cyclic polarization was shown in Fig. 3.

2.7. Analysis

The phase composition of the corrosion products were analyzed by X-ray diffraction (XRD), using a Bruker AXS D8 DISCOVER with GADDS. The D8 DISCOVER includes the third generation Goebel Mirrors providing the X-ray highest

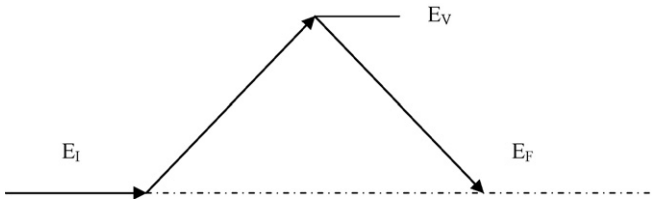

Fig. 3. The schematic diagram of the waveform of cyclic polarization.

flux density – essential for all thin film applications. High performance optics are selected and exchanged to provide the optimum resolution for each specimen. The microstructures and surface morphologies of the corrosion products were analyzed by FE-SEM, namely FEI Sirion 200. FEI Sirion 200 is an ultra-high resolution Schottky field emission scanning electron microscope and is ideal for studying materials on the nanometre scale. The microscope is equipped with Energy Dispersive Spectroscopy (EDS) system-Oxford Inca EDS.

3. Results

3.1. Immersion test

The microstructures and surface morphologies of the corrosion products of GW63K alloy in as-cast are shown in Fig. 4. The precipitation phase on the grain boundaries can be still identified clearly after immersing 10 min (Fig. 4a_1), however, it becomes difficult to identify the configurations of the grain boundaries after immersing 30 min and more long time (Fig. 4b_1 and c_1). Cracks were not observed on the surface of the film of corrosion products after immersing 10 and 30 min (Fig. 4a_2 and b_2). However, many cracks can be seen on the surface of the film of corrosion products after immersing 60 min (Fig. 4c_2). It can be clearly seen from Fig. 4(a_4, b_4 and c_4) that the morphologies of the film of corrosion products varied with immersion time. It is very similar to the honeycomb or sponge when the immersion time was 10 and 30 min, respectively. Moreover, the depth and wall thickness of the honeycomb are relatively lower and thinner after immersing 10 min than those after immersing 30 min. The morphology of the film of corrosion products changed from honeycomb into porous structure composed of tiny erect flaks after immersing 60 min. The result of XRD analysis indicated that the corrosion products of GW63K alloy in as-cast condition after immersing 10 h in 5 wt.% NaCl aqueous solution are mainly $Mg(OH)_2$ in addition to a little of $Gd(OH)_3$ (Fig. 5).

Fig. 6 shows the microstructures and surface morphologies of the corrosion products of GW63K alloy in T6 conditions. It was clearly shown that the presence of noble second phase particles influence strongly the distribution of pitting on GW63K alloy. It can be seen from Fig. 6(d_1 and e_1), namely lower magnification, that the corrosion prefer initiate from the nearest periphery of noble second phase particles to other places. The light, circular corrosion areas around the noble second phase particles gradually outspread with the increase of immersion time and the noble second phase particles falling away (Fig. 6f_1) from the substrate after immersing certain time (for example 60 min). The result of

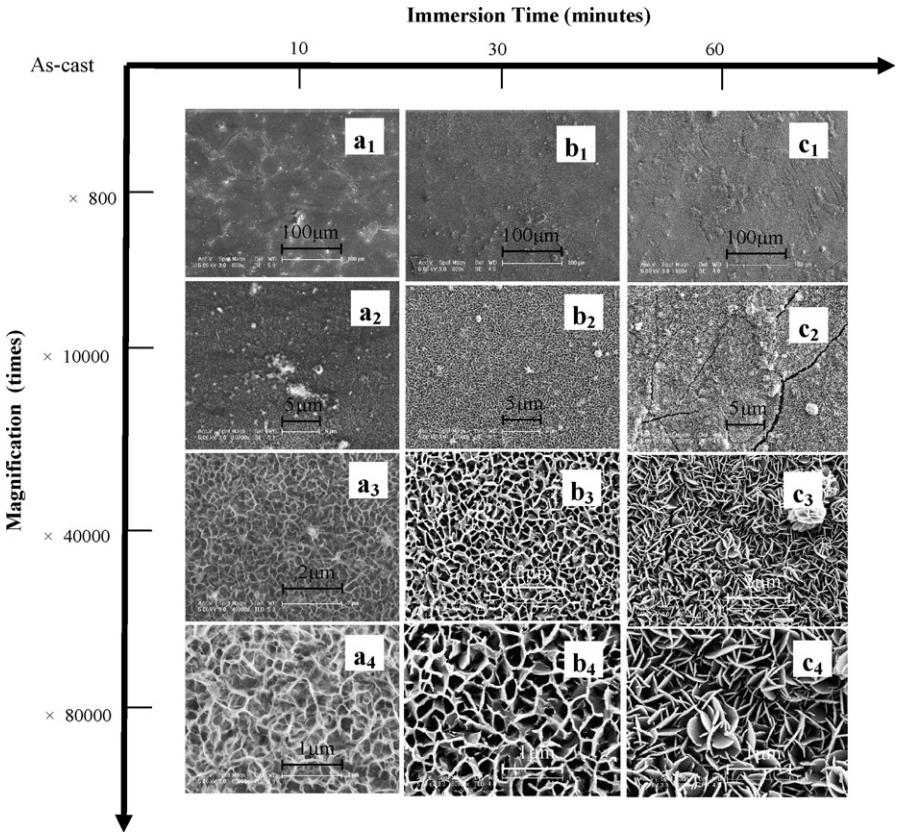

Fig. 4. The initiation and development of the corrosion products formed on the GW63K alloy in as-cast (a) after immersing 10 min, (b) 30 min and (c) 60 min.

EDS analysis indicated that the noble second phase particles are mainly compounds of (Mg–Gd–Y) and their hydroxide (Fig. 7). The result of XRD analysis shows that the corrosion products of GW63K alloy in T6 conditions after immersing 10 h in 5 wt.% NaCl aqueous solution are also mainly $Mg(OH)_2$ in addition to a little of $Gd(OH)_3$ (Fig. 8). However, the pure zirconium phase was no more found in the substrate alloy. The morphologies of the film of corrosion products also varied with immersion time as those in as-cast and also changed from honeycomb into porous structure composed of tiny erect flaks after immersing 60 min.

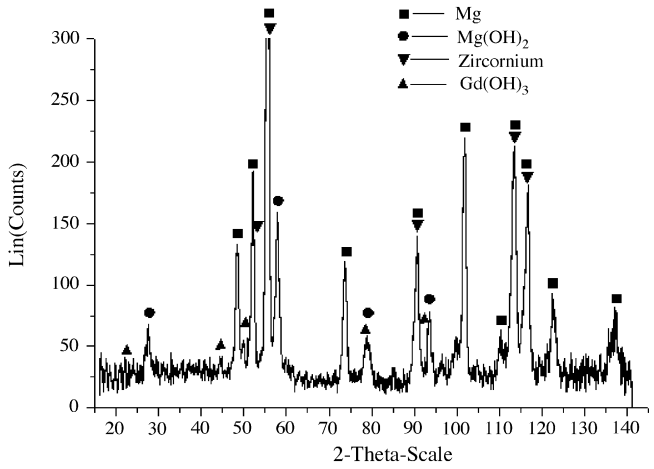

Fig. 5. The result of XRD analysis on the corrosion products of GW63K alloy in as-cast condition after immersing 10 h in 5 wt.% NaCl aqueous solution.

3.2. Open circuit potential measurements

The open circuit potentials (OCP) of the GW63K alloy in as-cast and T6 conditions were recorded for 1 h. Their evolutions with time are displayed in Fig. 9. The OCP increased from approximately −1.91 V to about −1.72 V in 25 min and their stabilization potential, namely the active state dissolution potentials (E_{CORR}) are −1.73 and −1.71 V, respectively, for both conditions.

3.3. Cyclic polarization (pitting scans)

The cyclic polarization curves of GW63K alloy in as-cast and T6 condition were shown in Fig. 10. On the forward scan curves, the corrosion potential of GW63K alloy in as-cast is about −1.71 V and that of it in T6 conditions is about −1.68 V, the latter being more positive than the former. On the reverse scan curves, the corrosion potentials of GW63K alloy in as-cast is about −1.74 V, in T6 is about −1.76 V. Both conditions shifted to a more negative value comparing to the forward scan. However, the value of difference in as-cast 0.03 V is smaller than 0.08 V in T6 condition.

3.4. EIS measurement

Fig. 11(a and b) show the EIS plots, measured at the E_{CORR}, on GW63K alloy immersed in 5 wt.% NaCl aqueous solutions. In the Nyquist plot two capacitive loops can be observed whether

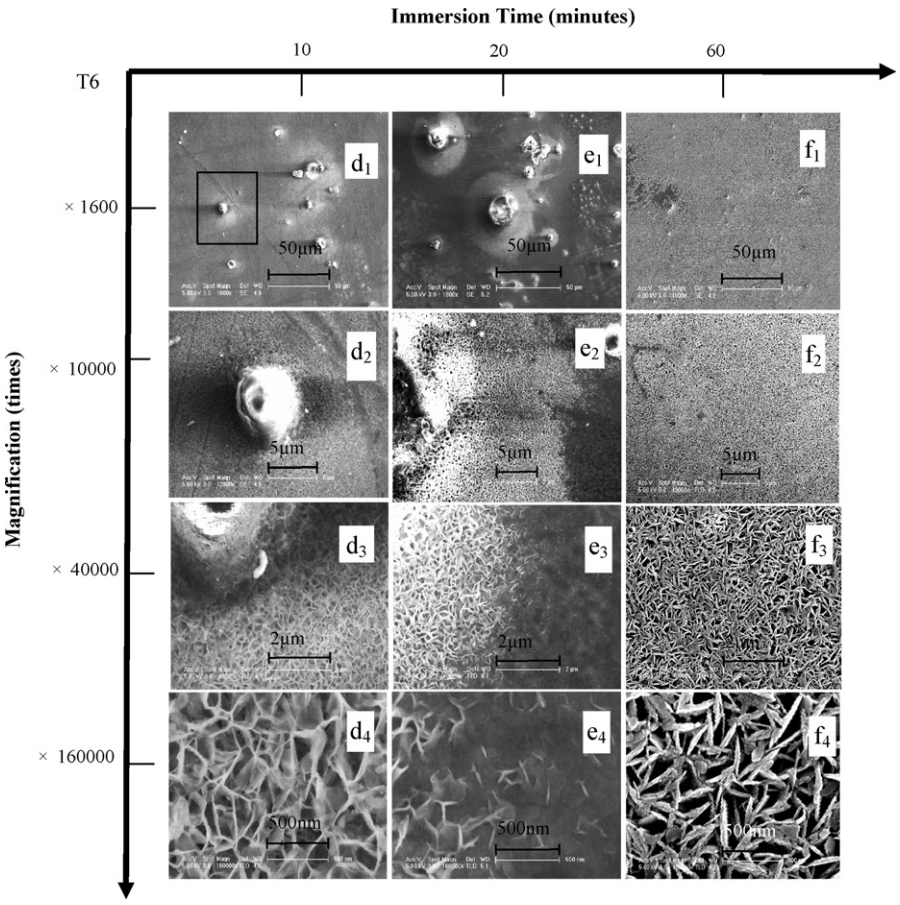

Fig. 6. The initiation and development of the corrosion products formed on the GW63K alloy in T6 condition (d) after immersing 10 min, (e) 20 min and (f) 60 min.

in as-cast or in T6 conditions, but the small loop was depressed to some degree for both of as-cast and T6 conditions. Their EIS spectra are similar except for the difference in diameter of the loops. The Bode plots demonstrate the presence of two time constants.

4. Discussion

The results of immersion test of GW63K alloy in as-cast indicated that the tensile stresses are existence in the film of corrosion products and increase with the growth of the film of corrosion products, namely with the increase of immersion time. The tensile stresses will ultimately result in cracking of the film of corrosion products after it reaches a critical value. It should be pointed out that it is difficult to distinguish the microstructure and morphologies of the film of corrosion products clearly if the magnification and resolution of the device of analysis are not high enough. This is why the ordinary SEM which we used in the early days on this work cannot clearly observe the details of the microstructures and morphologies of the corrosion products of GW63K alloys. The morphology and thickness of the film of corrosion products varied with immersion time. This change seems due to the walls of the honeycomb gradually grow and elongate from the trifurcate crunodes.

As far as the phase composition are concerned, in addition to the phases of $Mg(OH)_2$ and $Gd(OH)_3$, there are pure magnesium and zirconium phases in the result of XRD analysis on the corrosion products of GW63K alloy in as-cast condition. However, the pure magnesium and zirconium phases are belong to the substrate alloy. The existence of pure zirconium in the substrate coincide with the research results of references [1,2].

As it was pointed out by reference [17] that the investigators have been trying to explain the NDE phenomenon by means of electrochemical reaction mechanisms and four different mechanisms have been proposed for pure magnesium and its alloys. *Mechanism I* attributes the NDE to the breakdown of a partially protective film on the magnesium surface during anodic dissolution. *Mechanism II* explain the NDE in terms of the undermining and falling away of second phase particles during corrosion, especially at a higher anodic current density or potential. It is common for a particle to be undermined by the corrosion of the adjoining magnesium matrix and subsequently to fall out, result in a mass loss higher than that due to only electrochemical dissolution. *Mechanism III* believes that the monovalent magnesium ions may be involved as an intermediate species in the anodic dissolution process as the calculated valence of dissolved magnesium was reported in the range from 1.33 to 1.66. *Mechanism IV* believed that magnesium can be reduced to hydride by the following electrochemical reaction:

$$Mg + 2H^+ + 2e = MgH_2$$

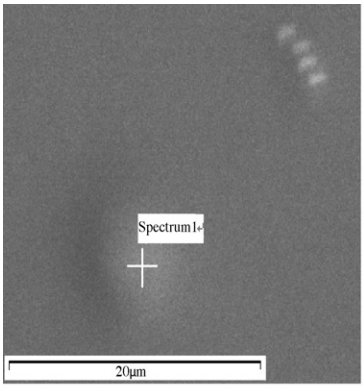

Element	App Conc.	Intensity Corrn.	Weight%	Weight% Sigma	Atomic%
O K	52.04	1.1843	33.53	0.81	45.00
Mg K	75.54	0.9417	61.17	0.89	54.02
Y L	1.65	0.5276	2.38	0.59	0.58
Gd L	3.01	0.7877	2.91	0.61	0.40
Totals			100.00		

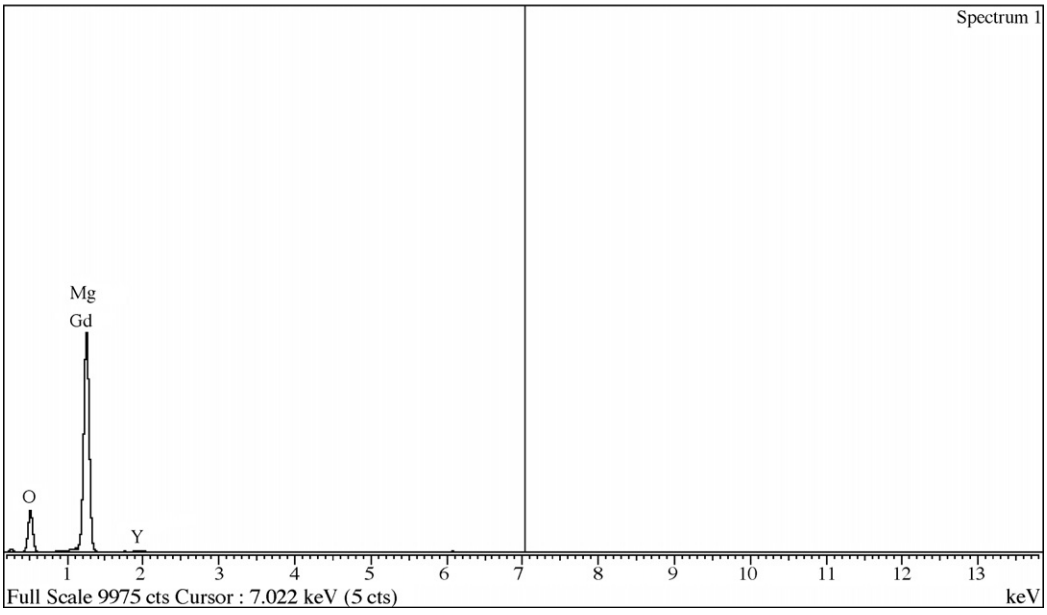

Fig. 7. The result of EDS analysis on the noble second phase particles.

The MgH_2 is not stable in contact with water and reacts chemically to form hydrogen:

$$MgH_2 + 2H_2O = Mg^{2+} + 2OH^- + 2H_2$$

This mechanism is based on thermodynamic data which predicts the stability of MgH_2.

The phenomena of noble second phase particles falling away (Fig. 6f$_1$) from the substrate after immersing certain time (for example 60 min) have been observed from the results of immersion test of GW63K alloy in T6 condition. This experimental result can be used as one of the evidences to support the *Mechanism II* explaining the mechanism of negative difference effect (NDE) phenomenon about magnesium and its alloys.

It should be noted that no chlorides are found in the film of corrosion products of GW63K alloy in both as-cast and T6 conditions based on the results of XRD analysis. As a result, the influences of Cl^- ions on the corrosion behavior of GW63K alloy in NaCl aqueous solutions are not demonstrated in this work and further research works are necessary to illustrate their roles.

It can be seen from Fig. 9 that the E_{CORR} value of GW63K alloy in T6 condition is little nobler than that in as-cast during all the test time. Perhaps this can be ascribed to the existence of more noble second phase particles such as the compounds of (Mg–Gd–Y) in T6 condition.

Generally, the cathodic polarization curves are assumed to represent the cathodic hydrogen evolution through water reduction, while the anodic ones represent the dissolution of magne-

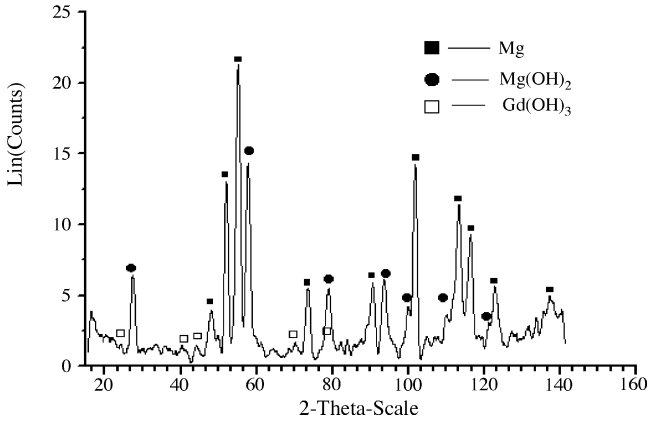

Fig. 8. The result of XRD analysis on the corrosion products of GW63K alloy in T6 conditions after immersing 10 h in 5 wt.% NaCl aqueous solution.

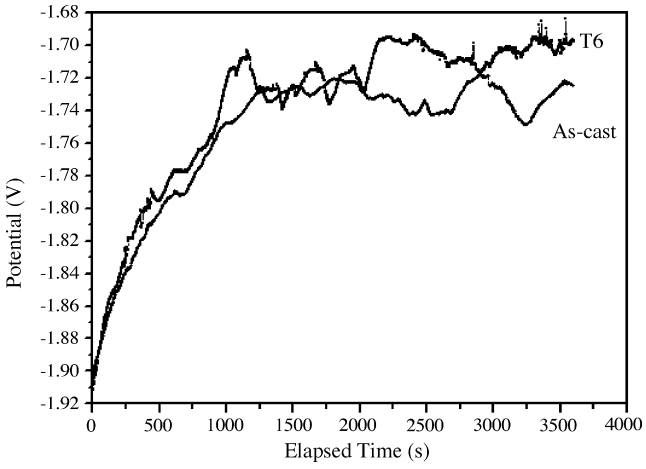

Fig. 9. The curve of open circuit potential vs. time of GW63 alloy in wt.% NaCl aqueous solution.

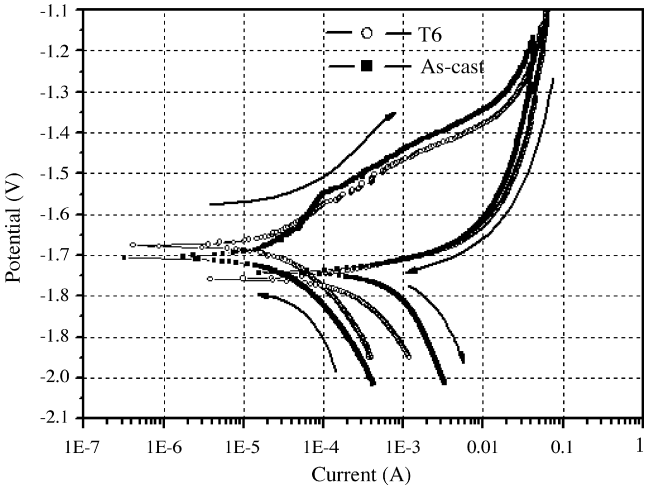

Fig. 10. Cyclic polarization curves of GW63K in as-cast and T6 condition.

sium. The cathodic parts of the curves in Fig. 10 indicate that the cathodic polarization current of hydrogen evolution reaction in T6 condition is higher than that in as-cast condition for GW63K alloy. This shows that the cathodic reaction is easier kinetically on the T6 specimen than that on the as-cast specimen. The anodic parts of the polarization curves in Fig. 10 reveal clearly the existence of a knee point (−1.63 to −1.65 V), which indicates the existence of some protective film, namely $Mg(OH)_2$, on the surface of the specimens. The growth rate of current densities becomes higher after the potential exceed the potential of the knee point and finally the obvious pitting appearance. Both of as-cast and T6 condition exhibit the same anodic curve-shape.

The forward scan curve to some extent represents the polarization behavior of the non-corrosion areas while the reverse scan curve is closely associated to the corroded areas of GW63K alloy. Due to the galvanic effect, an area with a more negative potential will be corroded and the area with a more positive potential will be protected. This means the corrosion in a corroding area on GW63K alloy whether in as-cast or in T6 conditions will be accelerated by the not corroded surrounding area and the surrounding area will be protected by the corrosion in the corroded area. As a result, the GW63K alloy has tendency to pit whether in as-cast or in T6 conditions and the tendency in T6 conditions is more serious than that in as-cast (Fig. 12). This also provides an explanation from an electrochemical point of view for the different corrosion appearance of GW63K alloy in as-cast and T6 condition when it was immersed in NaCl 5 wt.% aqueous solutions.

The EIS spectra for as-cast and T6 condition are similar except for the difference in diameter of the loops. This means that the corrosion mechanisms of the specimens in two conditions are similar, but their corrosion rates are different. The solution resistance is very low and can be ignored. The values of impedance at 0.1 Hz are about $10^3\ \Omega\ cm^2$ for as-cast and T6 condition (after immersion 1 h).

Based on the experimental results of immersion test, an equivalent electrical circuit was proposed to analyze the experimental data of EIS (Fig. 13). The honeycomb or porous characteristics of the corrosion products on the surface of the specimens and a charge transfer process in the pores are considered in the equivalent circuit. However, there are obvious errors existent when use the capacitance (C_{film}) of the film of corrosion products and the capacitance (C_{dl}) of double layer locating at the interface between the bottoms of the pores and the GW63K substrate to fit the experimental data. This means that the impedance behav-

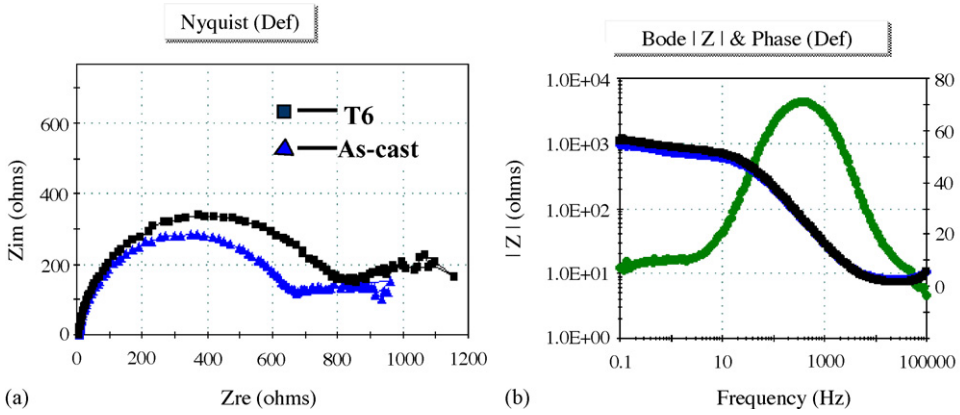

Fig. 11. (a and b) The Nyquist plots and Bode plots for GW63K in as-cast and T6 condition.

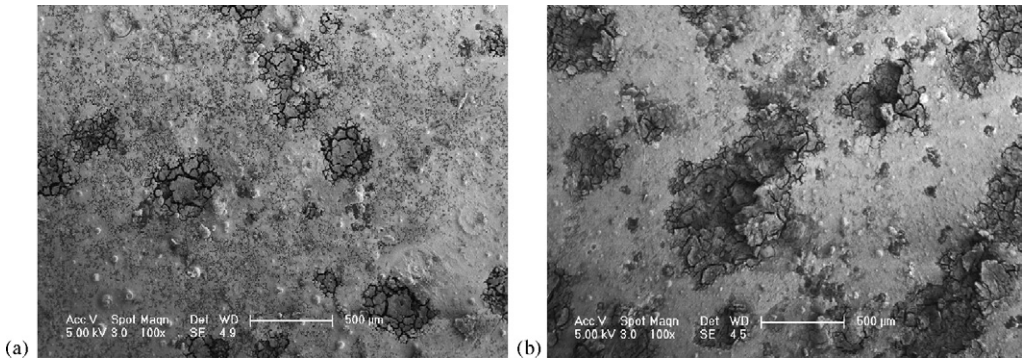

Fig. 12. The surface pitting appearances of GW63K alloy in (a) as-cast and (b) T6 condition after cyclic polarization test.

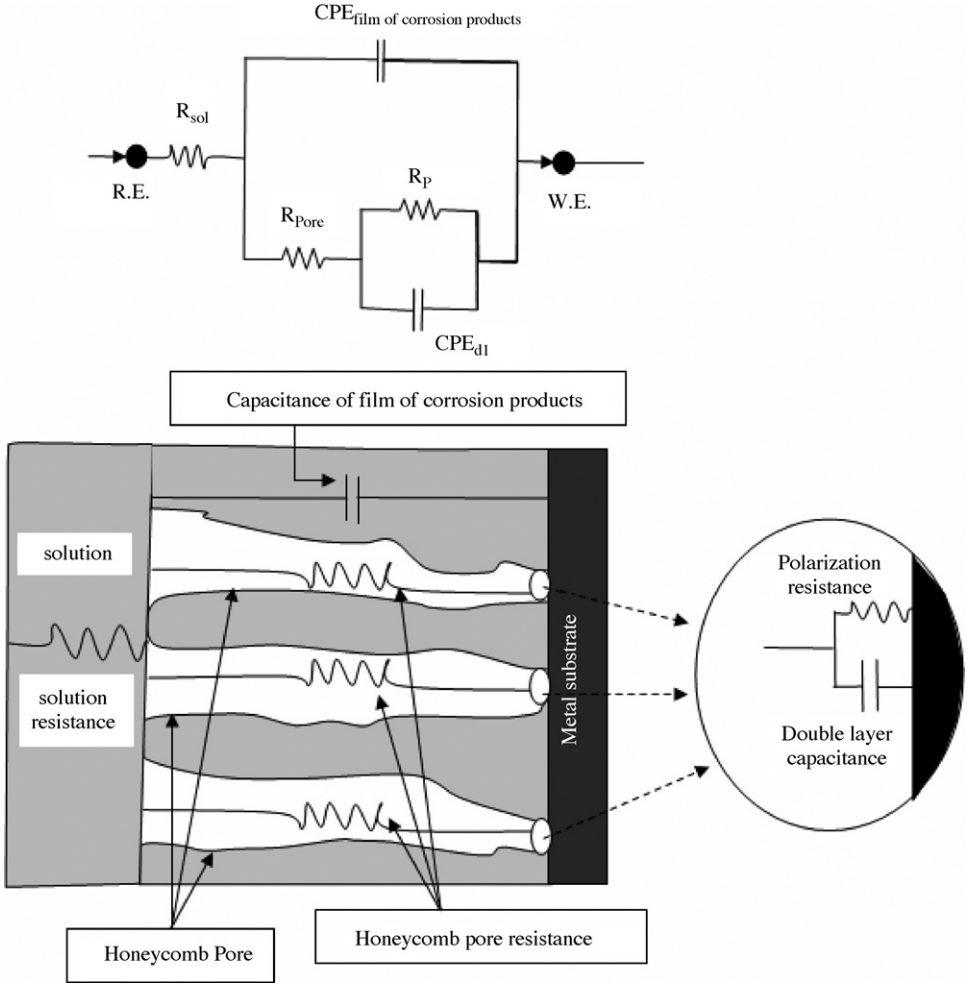

Fig. 13. Equivalent circuit model of fitting EIS data and circuit model of physical properties of the film of corrosion products.

Table 1
The values of the equivalent elements in the equivalent circuit

	R_{sol} ($\Omega\,cm^2$)	CPE_{film} ($S\,cm^{-2}\,s^{-1}$)	n_{film}	R_{pore} ($\Omega\,cm^2$)	CPE_{film} ($S\,cm^{-2}\,s^{-1}$)	n_{film}	R_p ($\Omega\,cm^2$)
As-cast	8.126	1.08E−5	0.9339	610.5	0.001586	0.5937	513.3
T6	10.24	2.344E−5	0.8867	1388	0.001402	0.8598	983.5

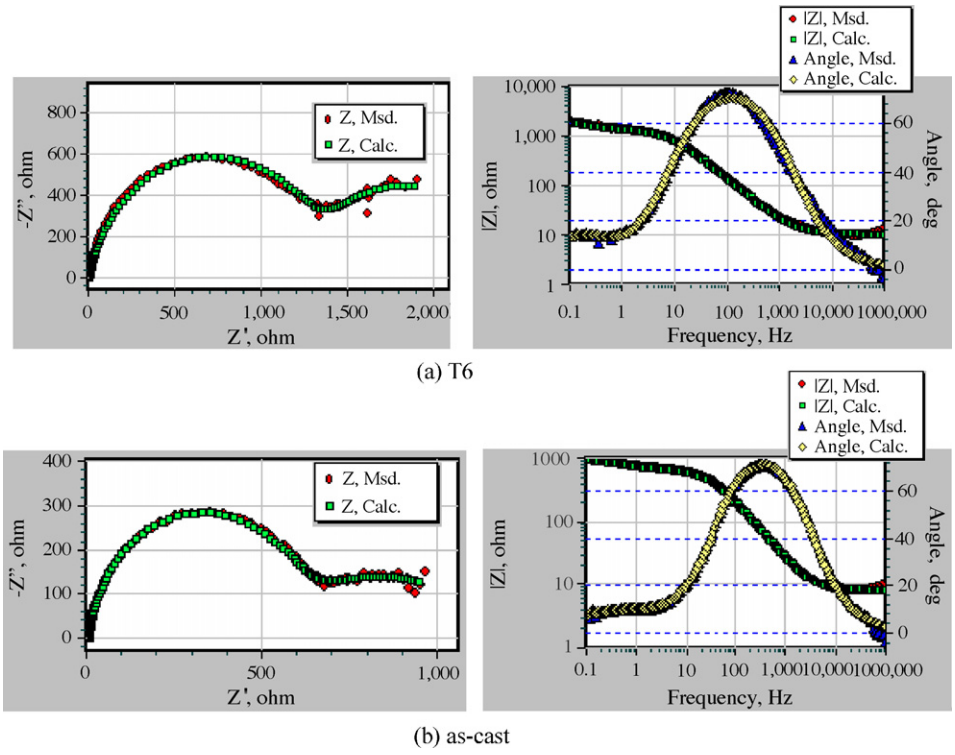

Fig. 14. The curves of experimental and simulated impedance data.

ior of the film of corrosion products is not completely consistent with that of the equivalent capacitance. In order to compensate the error, the constant phase elements (CPE) were considered in the equivalent circuit, where R_{sol} is the solution resistance; R_{pore} is the sum of the resistances of all pores in the film of corrosion products; CPE_{film} is the constant phase element representing the film of corrosion products; CPE_{dl} is the sum of constant phase elements of the double layers locating at the interface between the bottoms of the pores and the GW63K substrate. Very good agreement between the experimental and simulated data was found as is evident in Fig. 14(a and b). The simulation values obtained by *ZSimpWin* software for the equivalent elements are shown in Table 1.

5. Conclusions

Field emission scanning electron microscope (FE-SEM) was shown a valuable tool for investigating the microstructures and morphologies as well as the initiation and growth of the corrosion products formed on GW63K alloy. It was found that the morphologies of the film of corrosion products varied with immersion time and changed from honeycomb into porous structure composed of tiny erect flaks after immersing 60 min in 5 wt.% NaCl aqueous solution. The phenomena of undermining and falling away of the noble second phase particles for GW63K alloy in T6 condition can be used as an evidence to support the *Mechanism II* explaining the mechanism of negative difference effect about magnesium and its alloys.

It was indicated that the E_{CORR} of GW63K alloy in T6 conditions (−1.71 V) is little nobler than that in as-cast (−1.73 V). The test results of cyclic polarization show that GW63K alloy has tendency to pit whether in as-cast or in T6 conditions and the tendency in T6 condition is more serious than that in as-cast.

An equivalent circuit was proposed based on the EIS experimental data and the honeycomb or porous characteristics of the corrosion products formed on the surface of GW63K alloy. There are obvious errors existent when use the capacitance (C_{film}) of the film of corrosion products and the capacitance (C_{dl}) of double layer locating at the interface between the bottoms of the pores and the GW63K substrate to fit the experimental data. It is necessary for using the constant phase elements (CPE) to replace the correspondent capacitances in order to compensate the errors.

No mater whether GW63K alloy is in as-cast or in T6 condition the corrosion products formed on it in 5 wt.% NaCl aqueous solution are mainly $Mg(OH)_2$ in addition to a little of $Gd(OH)_3$. It should be noted that no chlorides were found in the film of corrosion products.

Future works will concentrate on improving the corrosion resistance and the tendency to pit for the magnesium alloys containing heavy rare earth (HRE) elements by adding alloying elements or carrying out heat treatment.

Acknowledgements

This work was in part supported by National Natural Science Foundation of China (50571047 and 5133003C). The authors thank Dr. Qun-Li Rao of the Center of Analysis and Measurement of Shanghai Jiao Tong University for assistance with the XRD and Dr. Zheng-Ming Ding and Dr. Yu-Jian Lai for assistance with the Field Emission Scanning Electron Microscope (FE-SEM).

References

[1] S.M. He, X.Q. Zeng, L.M. Peng, J. Alloys Compd. 427 (2007) 316–323.
[2] S.M. He, X.Q. Zeng, L.M. Peng, J. Alloys Compd. 421 (1–2) (2006) 309–313.
[3] B. Smola, et al., Mater. Sci. Eng. A 324 (2002) 113.
[4] I. Anthony, S. Kamado, Y. Kojima, Mater. Trans. 42 (2001) 1206.
[5] I. Anthony, S. Kamado, Y. Kojima, Mater. Trans. 42 (2001) 1212.
[6] P. Vostryi, et al., Phys. Stat. Sol. A 175 (1999) 491.
[7] L.L. Rokhlin, Proceedings of NATO Advanced Study Institute, Kluwer, 1998, p. 443.
[8] G.W. Lorimer, in: G.W. Lorimer (Ed.), Proceedings Magnesium Technology, Institute of Metals, London, 1986, p. 47.
[9] Y. Li, T. Zhang, W. Fuhui, Electrochim. Acta 51 (2006) 2845–2850.
[10] G. Song, Adv. Eng. Mater. 7 (7) (2005).
[11] G. Ballerini, U. Bardi, R. Bignucolo, G. Ceraolo, Corros. Sci. 47 (2005) 2173.
[12] G. Song, A.L. Bowles, D.H. St. John, Mater. Sci. Eng. A366 (2004) 74.
[13] S. Mathieu, C. Rapin, J. Steinmetz, P. Steinmetz, Corros. Sci. 45 (2003) 2741.
[14] R. Ambat, N.N. Aung, W. Zhou, Corros. Sci. 42 (2000) 1433.
[15] G. Song, A. Atrens, X. Wu, B. Zhang, Corros. Sci. 39 (09) (1998) 1769.
[16] R. Udhayan, D.P. Bhatt, J. Power Source 63 (1996) 103.
[17] G. Song, et al., Corros. Sci. 39 (5) (1997) 855.